the FEBS Journal

Hexameric ring structure of the N-terminal domain of *Mycobacterium tuberculosis* DnaB helicase

Tapan Biswas and Oleg V. Tsodikov

Department of Medicinal Chemistry, College of Pharmacy, University of Michigan, Ann Arbor, MI, USA

Keywords
crystal structure; DnaB helicase; primase; replication; tuberculosis

Correspondence
O. V. Tsodikov, Department of Medicinal Chemistry, College of Pharmacy, University of Michigan, Ann Arbor, MI 48109-1065, USA
Fax: +1 734 647 8430
Tel: +1 734 936 2676
E-mail: olegt@umich.edu

(Received 19 March 2008, revised 8 April 2008, accepted 11 April 2008)

doi:10.1111/j.1742-4658.2008.06460.x

Hexameric DnaB helicase unwinds the DNA double helix during replication of genetic material in bacteria. DnaB is an essential bacterial protein; therefore, it is an important potential target for antibacterial drug discovery. We report a crystal structure of the N-terminal region of DnaB from the pathogen *Mycobacterium tuberculosis* (*Mt*DnaBn), determined at 2.0 Å resolution. This structure provides atomic resolution details of formation of the hexameric ring of DnaB by two distinct interfaces. An extensive hydrophobic interface stabilizes a dimer of *Mt*DnaBn by forming a four-helix bundle. The other, less extensive, interface is formed between the dimers, connecting three of them into a hexameric ring. On the basis of crystal packing interactions between *Mt*DnaBn rings, we suggest a model of a helicase–primase complex that explains previously observed effects of DnaB mutations on DNA priming.

The *DnaB* gene encoding DnaB helicase was originally identified in a region of the bacterial genome, mutations in which caused a defect in DNA replication at elevated temperatures *in vivo* [1]. DnaB is an ATP-dependent helicase that unwinds parental duplex DNA during replication [2–5], thereby allowing the two strands to be copied. A hexamer of DnaB encircles the lagging strand and moves on it in the $5' \rightarrow 3'$ direction, thereby splitting the two complementary DNA strands [6]. A hexameric DnaB helicase alone is not very processive [7], whereas it becomes highly processive when bound to other replication proteins [8]. During DNA replication, DnaB is associated with multiple copies of DNA primase DnaG, which catalyzes the formation of RNA primers for the synthesis of Okazaki fragments on the lagging strand. The DnaB–DnaG complex plays a key role in coordinating the mechanistically different continuous and discontinuous DNA syntheses on the leading and the lagging strands, respectively [9].

A monomer of DnaB consists of two domains [10]: an N-terminal helical domain (DnaBn), shown to be required for formation of the functional helicase [11,12] and for binding DnaG [13], and a C-terminal RecA-like domain, responsible for DNA binding and ATP hydrolysis (Fig. 1A). Six monomers of DnaB form a two-tiered ring, as observed in recent modest-resolution structures of DnaB from the thermophilic *Geobacillus stearothermophilus* (*Gs*) [14], and in a low-resolution structure of a DnaB homolog G40P from *Bacillus subtilis* phage SPP1 [12], reported while this article was in preparation. One tier is formed by DnaBn, which has three-fold symmetry. The other tier is formed by the RecA-like ATPase domains in approximate six-fold symmetry. The hexameric composition of DnaB is shared by other representatives of the same superfamily of replicative helicases, such as bacteriophage T7 gene 4 protein [15], although significant differences in the sequence and domain organization exist among the family members.

DnaB helicase is conserved in the eubacterial kingdom, and is distinct from its functional relatives in higher eukaryotes. Therefore, DnaB is a very

Abbreviations
DnaBn, N-terminal helical domain of DnaB helicase; DnaGc, C-terminal domain of DnaG; *Gs*, *Geobacillus stearothermophilus*; HhH, helix–hairpin–helix (HhH); *Mt*, *Mycobacterium tuberculosis*.

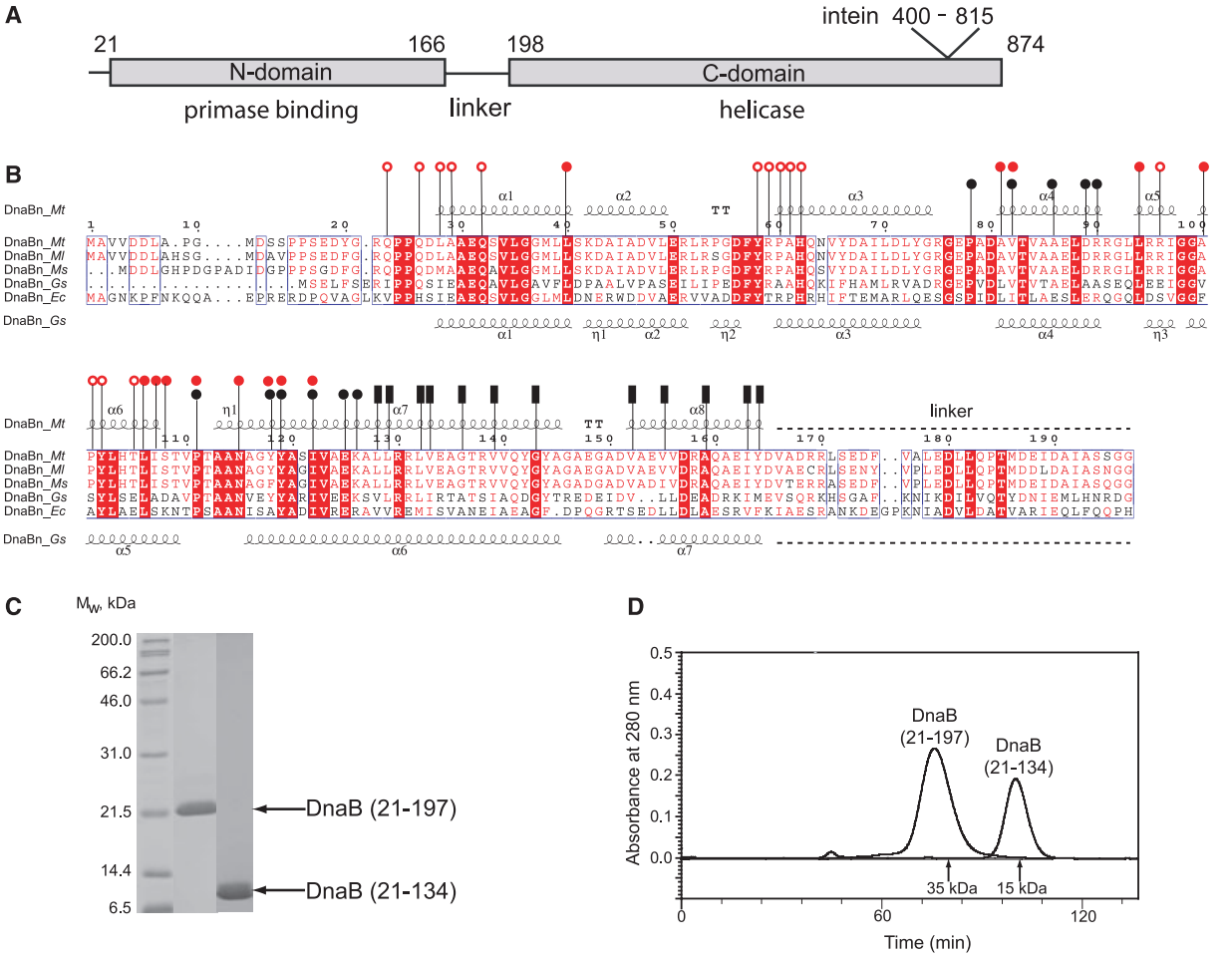

Fig. 1. (A) Domain organization of *Mt*DnaB. The numbers indicate approximate domain boundaries. The C-terminal domain of DnaB in *M. tuberculosis* and several other mycobacteria is disrupted by an intein, as indicated. (B) Sequence alignment of DnaBn. Sequences of DnaBn from several bacterial species (*Mt*, *M. tuberculosis*; *Ml*, *Mycobacterium leprae*; *Ms*, *Mycobacterium smegmatis*; *Gs*, *G. stearothermophilus*; *Ec*, *E. coli*) are aligned with the secondary structures of *Mt*DnaBn (above; this study) and *Gs*DnaBn [14]. The residues in the HhH–HhH interface of *Mt*DnaBn hexamer are indicated by black bars, and those in the dimer–dimer interface are indicated by black circles. The surface residues of *Mt*DnaB that form the putative DnaG-binding pocket (this study) are indicated by open red circles, and those of *Gs*DnaB that contact DnaG in the *Gs*DnaB–*Gs*DnaG structure [14] are indicated by filled red circles. (C) SDS/PAGE gel of purified *Mt*DnaB(21–197) and *Mt*DnaB(21–134) proteins. (D) A gel filtration chromatogram demonstrating that *Mt*DnaB(21–197) elutes as a dimer and *Mt*DnaB(21–134) as a monomer.

attractive target for antibacterial therapy. The C-terminal catalytic domain of DnaB is very highly conserved, which points at the conservation of the ATPase function in this helicase superfamily. DnaBn is less conserved, and its binding partner, the C-terminal domain of primase DnaG (DnaGc), is very weakly conserved. This divergence is intriguing, because it must be related to documented differences in intrinsic stabilities of DnaB–DnaG complexes between *Escherichia coli* and *G. stearothermophilus* [13,16–18]. This, in turn, implies divergent coordination of unwinding with priming at the replication fork in different bacteria.

We report a 2.0 Å resolution structure of the hexameric ring DnaBn from the pathogen *Mycobacterium tuberculosis* (*Mt*DnaBn). On the basis of the organization of the *Mt*DnaBn rings in the crystal lattice, we propose a model of the mycobacterial DnaB–DnaG complex.

Results and Discussion

Structure of the hexameric ring of *Mt*DnaBn

Bacterial DnaB helicase consists of two domains: the moderately conserved, entirely helical DnaBn (~ 24%

identity) (Fig. 1B) and the highly conserved C-terminal ATPase domain (~ 40% identity [19]). The two domains are connected by a linker region (Fig. 1A). In *M. tuberculosis* DnaB, *Mt*DnaBn (residues 21–197, including the linker) forms a stable dimer in solution (Fig. 1C,D). The region spanning residues 135–197 is required for dimer stability, because a truncated form of the protein (residues 21–134) is monomeric (Fig. 1C,D). *Mt*DnaBn forms a hexamer in the crystallization solution; the crystals of DnaBn contain one slightly asymmetric hexamer per asymmetric unit. Three two-fold symmetrical dimers of DnaBn are assembled into a hexamer that has approximate three-fold rotational symmetry (Fig. 2A). The two-fold and the three-fold symmetry axes are parallel to each other. The hexamer forms an opening in the shape of an equilateral triangle with a side length of 51 Å. Therefore, the ring can accommodate a cylinder with a maximum diameter of 34 Å, large enough for duplex and even triplex DNA. Indeed, DnaB is able to encircle and actively translocate on duplex DNA [20]. The triangular shape is roughly similar to one of the projections of electron microscopic structures of full-length *E. coli* DnaB hexamer [21]. Three monomers, one from each dimer, form the inner rim, and the other three monomers form the outer rim of the triangle. The backbones of all six monomers are generally very similar. There are subtle differences in the conformations of C-terminal helices α7 and α8 and in the hairpins connecting them (not shown). These differences indicate a small degree of conformational plasticity of the region closest to the mobile C-terminal domain of DnaB [14].

The interface stabilizing each dimer is formed between the C-terminal helix–hairpin–helix (HhH) regions of DnaBn (residues 128–165) that protrude from the globular subdomains (residues 21–127) (Fig. 2B). This explains our observation of the monomeric state of truncated DnaBn (residues 21–134). This interface is composed of conserved interdigitating hydrophobic residues (Figs 1B and 2B) that bury 2200 $Å^2$ of solvent-accessible surface area [22]. The C_α atoms of two glycine residues, Gly136 and Gly143, contribute to this interface and allow the helices

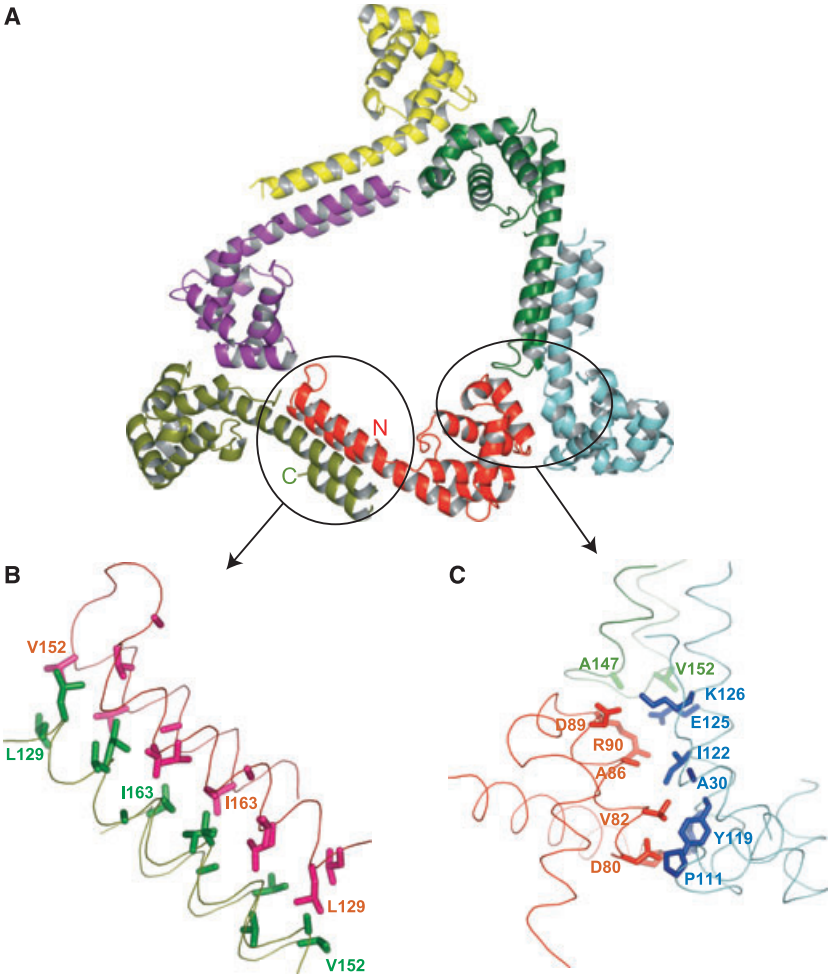

Fig. 2. The structure of the *Mt*DnaBn hexamer. (A) The hexameric ring of *Mt*DnaBn is shown as a ribbon diagram. (B) The HhH–HhH interface. (C) The dimer–dimer interface. In (B) and (C), the residues that form the respective interfaces (see also Fig. 1B) are shown as sticks, with a subset of them labeled.

to pack snugly against each other. DnaBs of other bacteria contain either a Gly or an Ala at these two positions. Previously reported mutations in *G. stearothermophilus* [23] and *Salmonella typhimurium* [24] DnaB that cause a priming defect (Val133 and Val139 in *Mt*DnaB) lie in this hydrophobic interface. These substitutions are likely to abolish DnaB–DnaG binding by disrupting the structure of DnaBn. The solvent-exposed residues of the HhH are generally not conserved. The entire HhH region is required for dimerization, because the slightly shorter DnaBn of *E. coli* (residues 1–161, homologous to residues 1–159 of *Mt*DnaB[25]) is monomeric. Indeed, residues Ile163 and Tyr164 of *Mt*DnaBn, close to the end of the structured region, are located in the dimerization interface (Fig. 1B). The linker (residues 167–197) is not found in the electron density, consistent with its conformational flexibility [14]. This flexibility accommodates large movements of the C-terminal catalytic domains relative to each other and to the N-terminal tier [14].

The interface between the dimers is much less extensive (1020 $Å^2$ of buried surface area), which explains the lower stability of dimer–dimer interactions (Fig. 2C). It is formed predominantly by a set of hydrophobic contacts between the two globular subdomains. In addition, this interface contains two salt bridges, Arg90–Glu125 and Asp89–Lys126, between the globular subdomain of an inner monomer and the HhH subdomain of an outer monomer. Mutations in this interface significantly reduce the helicase activity of the DnaB homolog G40P [12]. The residues in the dimer–dimer interface are generally, but not universally, conserved (Fig. 1B).

The inner surface of the DnaBn ring contains three positively charged patches, each formed by Arg90, Arg91, Arg 95, and Arg96 (Fig. 3A), that may bind the lagging DNA strand during replication. These arginines are conserved in mycobacteria, but not in other bacteria (Fig. 1B). Bailey *et al.* [14] proposed that ssDNA binds inside the ring at a different site (Fig. 3C), formed by side chains of Arg116, Arg117 and Arg120 of *Gs*DnaB. Among these residues, only Arg116 is conserved (Fig. 1B). The lagging DNA strand must be positioned inside the DnaB ring somewhat differently in different prokaryotes. Such differential positioning is likely to be related to concomitant differences in the DnaB–DnaG interface (see the next section). The surface residues of DnaB facing the center of the ring and the N-terminal side are dramatically different for *Mt*DnaB and *Gs*DnaB (Fig. 3A,C). In contrast, the surface facing the ATPase domain is highly conserved and uniformly negatively charged (Fig. 3B,D). This conservation must preserve the nature of interactions between the N-terminal and the C-terminal domains of DnaB in different bacteria.

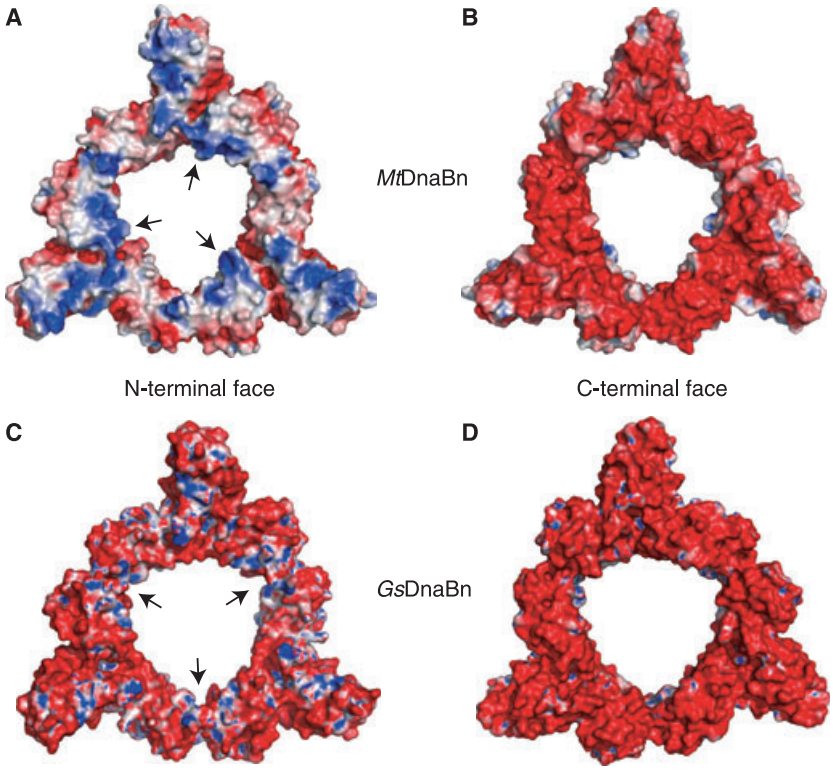

Fig. 3. The electrostatic surface of *Mt*DnaBn and *Gs*DnaBn. The positive surface is shown in blue and the negative surface in red. The sides facing the C-terminal domain (B, D) in *Mt*DnaBn (A, B) (this study) and *Gs*DnaBn rings (C, D) [14] are similar, whereas the N-terminal faces (A, C) are drastically different. The proposed binding sites for the lagging DNA strand are indicated by the arrows.

A model of the helicase–primase complex

DnaBn and its binding partner, DnaGc, are structurally similar [10,14,16,26–29]. Therefore, we considered the possibility that DnaBn from one hexamer would mimic binding of DnaGc to another hexamer of DnaBn in the crystal lattice. Indeed, in our crystal structure, three DnaBn monomers are bound to the N-terminal face of each hexameric ring (Fig. 4). This 6 : 3 DnaB–DnaG stoichiometry was observed in solution [13]. Binding of each *Mt*DnaBn monomer (DnaGc mimic) to the hexameric ring buries 1900 Å of solvent-accessible surface area. This interface is different from those observed in dimeric structures of the globular subdomain of *E. coli* DnaBn [27,28]. The binding surface of the proposed DnaGc mimic involves the C-terminal helix (the DnaG counterpart of helix α8 in DnaBn). DnaG mutations in this helix were shown to be disruptive to the DnaB–DnaG complex [30]. Each DnaGc mimic is bound to the globular subdomains of inner and outer monomers across the dimer–dimer interface, thereby stabilizing the hexameric ring of DnaB. Such bidentate interaction is consistent with the role of DnaG in contributing to the stability of the hexamer of DnaB and stimulating its activity [5]. N-terminal truncations of the globular subdomain of DnaBn were reported to abolish helicase–primase interactions [12], in agreement with our structural model. In the structure of the *Gs*DnaB–*Gs*DnaGc complex [14], DnaGc also binds across the dimer–dimer interface of DnaBn and comparably buries 2500 Å of surface area. However, *Gs*DnaGc is bound to a different surface of the *Gs*DnaBn ring (Figs 4 and 1B). In an elegant study, Chang & Marians [31] demonstrated that the *E. coli* DnaB mutations Glu32 → Lys (Ala29 in *M. tuberculosis* and either a Glu or an Ala in other bacteria) and Tyr105 → Ala (Tyr102 in *M. tuberculosis*; almost universally conserved) increase the Okazaki fragment size by destabilizing the DnaB–DnaG association. No effect was observed for the Glu32 → Ala mutation. In a different system, *Gs*DnaB mutation Tyr88 → Ala (Tyr105 in *E. coli*) was disruptive to the DnaB–DnaG complex, whereas the Glu15 → Ala (Glu32 in *E. coli*) mutation was not [23]. These mutagenesis studies are in excellent agreement with our model of the DnaB–DnaG complex: both of these residues are located directly in the putative DnaB–DnaG interface (Figs 4 and 1B). Intriguingly, these two DnaB residues do not make direct contacts with DnaG in the *Gs*DnaB–*Gs*DnaG structure [14] (see also Fig. 4).

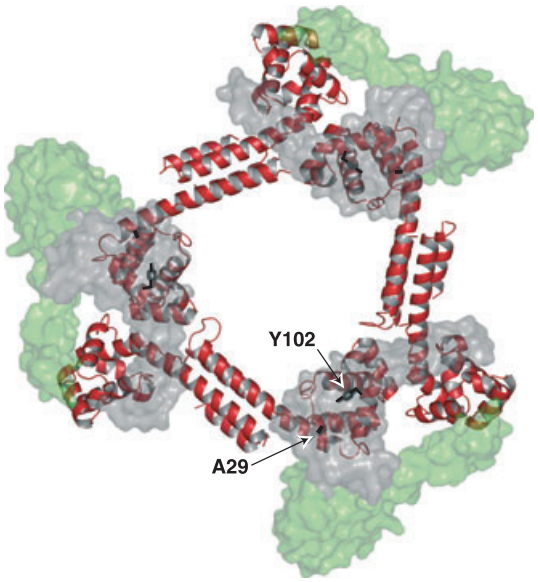

Fig. 4. The model of the DnaB–DnaG complex. *Mt*DnaBn monomers that mimic DnaGc are shown as the semitransparent gray surface. *Gs*DnaGc (in green) from the *Gs*DnaB–*Gs*DnaGc complex [14] is shown for comparison. The DnaB residues critical for priming (Ala29 and Tyr102; see text) are shown as sticks.

The two distinct positions of DnaG on the DnaB ring need not be mutually exclusive. *E. coli* DnaG priming activity was demonstrated to be distributive because of the relatively weak association of DnaG with DnaB. More than one position of DnaG on DnaB during replication (e.g. in the idle and in the actively priming states) would be consistent with these observations. Alternatively, DnaGc may bind DnaBn somewhat differently in different bacteria. This possibility is strengthened by poor conservation of DnaGc [29] and the N-terminal face residues of the DnaBn ring (Fig. 3A,C). Testing these structural and mechanistic proposals is a subject of future research in this laboratory.

Conclusions

In summary, we have obtained a high-resolution structure of the hexameric ring formed by the *Mt*DnaBn. The stable dimers of DnaBn have a propensity for trimerization in the absence of DnaGc. The structure provides the highest-resolution view of the interactions essential for hexamer stability, and suggests a model for the DnaB–DnaG complex that is consistent with previous mutagenesis studies.

Experimental procedures

Cloning, protein expression, and purification

The DnaB constructs (locus tag Rv0058; residues 21–197 and residues 21–134) from *Mycobacterium tuberculosis* H37Rv were amplified by PCR from genomic DNA, and ligated

between the *Nde*I and *Xho*I sites of the modified pET19b (EMD Biosciences, San Diego, CA, USA) with an N-terminal decahistidine tag separated from the gene by the Prescission protease (GE Healthcare, Piscataway, NJ, USA) cleavage site. The proteins were expressed in BL21(DE3) *E. coli* cells that were initially grown in LB supplemented with 100 $\mu g \cdot mL^{-1}$ ampicillin at 37 °C until the culture reached an attenuance (D) at 600 nm of 0.4–0.6. Then, the culture was induced with 0.5 mM isopropyl thio-β-D-galactoside at 19 °C overnight. The cells were harvested by centrifugation at 5000 ***g*** for 10 min, resuspended, and lysed by sonication in lysis buffer (40 mM Tris, pH 8.0, 400 mM NaCl, 10% glycerol, 2 mM β-mercaptoethanol). The clarified lysate was passed through an IMAC (GE Healthcare) Ni^{2+} column, following the manufacturer's instructions. The tag was cleaved with Prescission protease (GE Healthcare) overnight at 4 °C. The protein was then concentrated using an Amicon Ultra-15 centrifugal filter unit (Millipore, Bellerica, MA, USA) and purified further on an S-200 size exclusion column (GE Healthcare) equilibrated in 40 mM Tris, pH 8.0, 200 mM NaCl, 2 mM β-mercaptoethanol and 0.1 mM EDTA. Fractions containing DnaBn were pooled, and concentrated to 10 $mg \cdot mL^{-1}$ using an Amicon Ultra-15 centrifugal filter unit. The concentrated protein was used for crystallization.

Protein crystallization, data collection, and structure determination and refinement

Initial high-throughput crystallization screening of *Mt*DnaBn was performed at the Hauptman–Woodward Institute [32]. Single crystals of size 0.1 × 0.1 × 0.1 mm were grown in 4–6 weeks by microbatch crystallization in mineral oil at 21 °C. The drops contained a mixture of 1 μL of the concentrated protein (see above) and 1 μL of crystallization solution. Crystallization solution consisted of 100 mM citrate sodium salt (we used a stock solution of 1 M citric acid adjusted to pH 4.0 with 1 M sodium citrate), 100 mM dibasic potassium phosphate, and 17.5% poly(ethylene glycol) 8000. The crystals were gradually transferred to crystallization solution with 16.5% glycerol, incubated overnight, and then flash frozen in liquid nitrogen. X-ray diffraction data were collected at 100 K at LS-CAT beamline (sector 21-ID) at the Advanced Photon Source at the Argonne National Laboratory. The diffraction data were processed using the HKL2000 suite [33]. The crystals were not merohedrally twinned [34]. The structure of *Mt*DnaBn was determined by molecular replacement using program PHASER [35], with residues 5–112 of the monomeric DnaB from *Thermus aquaticus* [10] as a search model. The missing part of the structure was then built into the unambiguous F_o–F_c electron density. The structure of *Mt*DnaBn was iteratively rebuilt and refined by using programs COOT [36] and REFMAC [37], respectively, to a final resolution of 2.0 Å. The data collection and refinement statistics are given in Table 1. The structure and the diffraction data were deposited in the Protein Data Bank (code: 2r5u).

Table 1. Crystallographic data collection and structure refinement statistics.

Data collection	
Space group	$P3_1$
Cell dimensions	
$a/b/c$ (Å)	114.9/114.9/72.4
$\alpha/\beta/\gamma$ (°)	90/90/120
Composition	Six monomers per asymmetric unit
Resolution	50.0–2.0 (2.06–2.00)[a]
R_{merge}	0.083 (0.64)
$I/\sigma I$	12.2 (2.0)
Completeness	0.99 (0.95)
Redundancy	5.5 (4.1)
Refinement	
Resolution (Å)	30.0–2.0 (2.05–2.00)
No. of reflections	67 873 (3634)
R/R_{free}	0.23/0.28 (0.30/0.35)
No. of atoms	
Protein	6429
Water	421
rmsd	
Bond lengths (Å)	0.011
Bond angles (°)	1.23

[a] The highest-resolution-shell values are shown in parentheses.

Acknowledgements

We thank Dr Nick Dixon for helpful discussions on the manuscript.

The research was supported by start-up funds to O. V. Tsodikov from the College of Pharmacy at the University of Michigan. We would like to thank the staff of LS-CAT, and especially Spencer Anderson, for assistance with the data collection at the APS.

References

1 Hirota Y, Ryter A & Jacob F (1968) Thermosensitive mutants of *E. coli* affected in the processes of DNA synthesis and cellular division. *Cold Spring Harb Symp Quant Biol* **33**, 677–693.

2 LeBowitz JH & McMacken R (1986) The *Escherichia coli* dnaB replication protein is a DNA helicase. *J Biol Chem* **261**, 4738–4748.

3 Baker TA, Sekimizu K, Funnell BE & Kornberg A (1986) Extensive unwinding of the plasmid template during staged enzymatic initiation of DNA replication from the origin of the *Escherichia coli* chromosome. *Cell* **45**, 53–64.

4 Schaeffer PM, Headlam MJ & Dixon NE (2005) Protein–protein interactions in the eubacterial replisome. *IUBMB Life* **57**, 5–12.

5 Corn JE & Berger JM (2006) Regulation of bacterial priming and daughter strand synthesis through

helicase–primase interactions. *Nucleic Acids Res* **34**, 4082–4088.
6 Kaplan DL (2000) The 3′-tail of a forked-duplex sterically determines whether one or two DNA strands pass through the central channel of a replication-fork helicase. *J Mol Biol* **301**, 285–299.
7 Galletto R, Jezewska MJ & Bujalowski W (2004) Unzipping mechanism of the double-stranded DNA unwinding by a hexameric helicase: quantitative analysis of the rate of the dsDNA unwinding, processivity and kinetic step-size of the *Escherichia coli* DnaB helicase using rapid quench-flow method. *J Mol Biol* **343**, 83–99.
8 Mok M & Marians KJ (1987) The *Escherichia coli* preprimosome and DNA B helicase can form replication forks that move at the same rate. *J Biol Chem* **262**, 16644–16654.
9 Tanner NA, Hamdan SM, Jergic S, Schaeffer PM, Dixon NE & van Oijen AM (2008) Single-molecule studies of fork dynamics in *Escherichia coli* DNA replication. *Nat Struct Mol Biol* **15**, 170–176.
10 Bailey S, Eliason WK & Steitz TA (2007) The crystal structure of the *Thermus aquaticus* DnaB helicase monomer. *Nucleic Acids Res* **35**, 4728–4736.
11 Biswas SB, Chen PH & Biswas EE (1994) Structure and function of *Escherichia coli* DnaB protein: role of the N-terminal domain in helicase activity. *Biochemistry* **33**, 11307–11314.
12 Wang G, Klein MG, Tokonzaba E, Zhang Y, Holden LG & Chen XS (2008) The structure of a DnaB-family replicative helicase and its interactions with primase. *Nat Struct Mol Biol* **15**, 94–100.
13 Bird LE, Pan H, Soultanas P & Wigley DB (2000) Mapping protein–protein interactions within a stable complex of DNA primase and DnaB helicase from *Bacillus stearothermophilus*. *Biochemistry* **39**, 171–182.
14 Bailey S, Eliason WK & Steitz TA (2007) Structure of hexameric DnaB helicase and its complex with a domain of DnaG primase. *Science* **318**, 459–463.
15 Singleton MR, Sawaya MR, Ellenberger T & Wigley DB (2000) Crystal structure of T7 gene 4 ring helicase indicates a mechanism for sequential hydrolysis of nucleotides. *Cell* **101**, 589–600.
16 Oakley AJ, Loscha KV, Schaeffer PM, Liepinsh E, Pintacuda G, Wilce MC, Otting G & Dixon NE (2005) Crystal and solution structures of the helicase-binding domain of *Escherichia coli* primase. *J Biol Chem* **280**, 11495–11504.
17 Lu YB, Ratnakar PV, Mohanty BK & Bastia D (1996) Direct physical interaction between DnaG primase and DnaB helicase of *Escherichia coli* is necessary for optimal synthesis of primer RNA. *Proc Natl Acad Sci USA* **93**, 12902–12907.
18 Thirlway J, Turner IJ, Gibson CT, Gardiner L, Brady K, Allen S, Roberts CJ & Soultanas P (2004) DnaG interacts with a linker region that joins the N- and C-domains of DnaB and induces the formation of 3-fold symmetric rings. *Nucleic Acids Res* **32**, 2977–2986.
19 Leipe DD, Aravind L, Grishin NV & Koonin EV (2000) The bacterial replicative helicase DnaB evolved from a RecA duplication. *Genome Res* **10**, 5–16.
20 Kaplan DL & O'Donnell M (2002) DnaB drives DNA branch migration and dislodges proteins while encircling two DNA strands. *Mol Cell* **10**, 647–657.
21 San Martin MC, Stamford NP, Dammerova N, Dixon NE & Carazo JM (1995) A structural model for the *Escherichia coli* DnaB helicase based on electron microscopy data. *J Struct Biol* **114**, 167–176.
22 Tsodikov OV, Record MT Jr & Sergeev YV (2002) Novel computer program for fast exact calculation of accessible and molecular surface areas and average surface curvature. *J Comput Chem* **23**, 600–609.
23 Thirlway J & Soultanas P (2006) In the *Bacillus stearothermophilus* DnaB–DnaG complex, the activities of the two proteins are modulated by distinct but overlapping networks of residues. *J Bacteriol* **188**, 1534–1539.
24 Stordal L & Maurer R (1996) Defect in general priming conferred by linker region mutants of *Escherichia coli* dnaB. *J Bacteriol* **178**, 4620–4627.
25 Miles CS, Weigelt J, Stamford NP, Dammerova N, Otting G & Dixon NE (1997) Precise limits of the N-terminal domain of DnaB helicase determined by NMR spectroscopy. *Biochem Biophys Res Commun* **231**, 126–130.
26 Syson K, Thirlway J, Hounslow AM, Soultanas P & Waltho JP (2005) Solution structure of the helicase-interaction domain of the primase DnaG: a model for helicase activation. *Structure* **13**, 609–616.
27 Fass D, Bogden CE & Berger JM (1999) Crystal structure of the N-terminal domain of the DnaB hexameric helicase. *Structure* **7**, 691–698.
28 Weigelt J, Brown SE, Miles CS, Dixon NE & Otting G (1999) NMR structure of the N-terminal domain of *E. coli* DnaB helicase: implications for structure rearrangements in the helicase hexamer. *Structure* **7**, 681–690.
29 Su XC, Schaeffer PM, Loscha KV, Gan PH, Dixon NE & Otting G (2006) Monomeric solution structure of the helicase-binding domain of *Escherichia coli* DnaG primase. *FEBS J* **273**, 4997–5009.
30 Tougu K & Marians KJ (1996) The extreme C terminus of primase is required for interaction with DnaB at the replication fork. *J Biol Chem* **271**, 21391–21397.
31 Chang P & Marians KJ (2000) Identification of a region of *Escherichia coli* DnaB required for functional interaction with DnaG at the replication fork. *J Biol Chem* **275**, 26187–26195.
32 Luft JR, Collins RJ, Fehrman NA, Lauricella AM, Veatch CK & DeTitta GT (2003) A deliberate

approach to screening for initial crystallization conditions of biological macromolecules. *J Struct Biol* **142**, 170–179.
33 Otwinowski Z & Minor W (1997) Processing of X-ray diffraction data collected in oscillation mode. *Macromolec Crystallogr A* **276**, 307–326.
34 Yeates TO (1997) Detecting and overcoming crystal twinning. *Methods Enzymol* **276**, 344–358.
35 Mccoy AJ, Grosse-Kunstleve RW, Adams PD, Winn MD, Storoni LC & Read RJ (2007) Phaser crystallographic software. *J Appl Crystallogr* **40**, 658–674.
36 Emsley P & Cowtan K (2004) Coot: model-building tools for molecular graphics. *Acta Crystallogr D Biol Crystallogr* **60**, 2126–2132.
37 Murshudov GN, Vagin AA & Dodson EJ (1997) Refinement of macromolecular structures by the maximum-likelihood method. *Acta Crystallogr D Biol Crystallogr* **53**, 240–255.